

Intercalation Mechanisms of Fe Atoms underneath A Graphene Monolayer on Ru(0001)

Peng Zhao,^{†,‡,§,||} Pengju Ren,^{†,‡,¶} C. J. Kees-Jan Weststrate,^{⊥,¶} Yuqun Xu,[§] Dong-Bo Cao,^{†,‡} Hongwei Xiang,^{†,‡,§} Jian Xu,^{‡,§} Yong Yang,^{†,‡,§} Yong-Wang Li,^{†,‡,§} J. W. Hans Niemantsverdriet,^{§,⊥} Xiaodong Wen,^{*,†,‡,§,¶} and Xin Yu^{*,†,‡,§,¶}

[†]State Key Laboratory of Coal Conversion, Institute of Coal Chemistry, Chinese Academy of Sciences, Taiyuan 030001, China

[‡]National Energy Center for Coal to Liquids, Synfuels China Co., Ltd., Huairou District, Beijing 101400, China

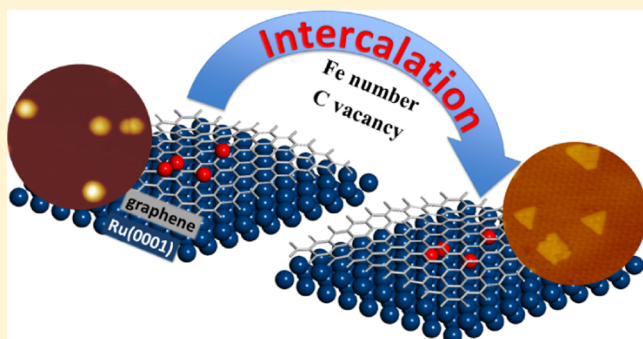
[§]SynCat@Beijing, Synfuels China Technology Co. Ltd., Leyuan South Street II, No. 1, Huairou District, Beijing 101407, China

[¶]University of Chinese Academy of Sciences, No. 19A Yuquan Road, Beijing 100049, China

^{*}SynCat@DIFFER, Syngaschem BV, P.O. Box 6336, Eindhoven 5600 HH, The Netherlands

Supporting Information

ABSTRACT: The intercalation process of iron atoms in the interface between graphene and Ru(0001) was systematically investigated both experimentally and computationally. Scanning tunneling microscopy and low-energy electron diffraction indicate that Fe intercalates at 700 K in the graphene/Ru(0001) system, where the graphene monolayer covers the whole substrate. An atomic-level understanding of the process is achieved using dispersion-corrected density functional theory (DFT) calculation. The results indicate that single-Fe atom intercalation causes only minor energy changes in the system. In contrast, the intercalation of a Fe dimer leads to a considerable drop in the total energy, more than twice the energy change in the case of the single-atom intercalation. In a sequential process, intercalation of the second Fe releases more energy, indicating that once the initial intercalation occurs, the subsequent process is thermodynamically more favored than the first. Combining the experimental observations with theoretical insights from the DFT calculations, we provide a clear picture of Fe intercalation into graphene/Ru(0001), which we believe is of interest to the field of interface and materials science and catalysis.



1. INTRODUCTION

Graphene has been widely studied both experimentally and computationally to understand its physical and chemical properties owing to its potential for applications in electronic devices.^{1–3} In addition, graphene grown on a metal substrate can be considered as mono- or multilayer graphite coke, which is known as a catalyst poison, suppressing catalytic activity by blocking the active sites of the metal catalyst.^{4–7} The study of graphene grown on metal substrates may therefore give useful information on catalytic reactions involving hydrocarbons, such as Fischer–Tropsch synthesis.⁸ The interface between graphene and the underlying metal surface plays an important role in the preparation of large-scale graphene on metal substrates^{9,10} and graphene-based spintronic units.^{11,12} In addition, the properties of epitaxial graphene/substrate interfaces are strongly dependent on the materials inserted between graphene and support.^{13–16} For instance, intercalation of ferromagnets between graphene and metal substrate would possibly allow the preparation of arrays of magnetic nanostructures, whose shape and size are strongly influenced by the intricate spatial binding strength variation at the

graphene/substrate interface.¹⁷ Sutter et al.¹⁸ demonstrated the controlled modification of a macroscopic graphene–metal interface by oxygen intercalation.

However, to date, it is not clear how intercalation happens in graphene/substrate systems, although various possible intercalation mechanisms, such as “exchange intercalation mechanism”,¹⁹ “intercalation through defects”,²⁰ “penetration from surface steps”,²¹ and “intercalation through metal-generated defects”,¹⁷ have been considered. Density functional theory (DFT) calculations suggest a Si–C exchange mechanism facilitates the penetration of Si at the graphene/Ru(0001) interface.¹⁹ Jin et al.²¹ studied the intercalation of Pb atoms at the graphene/Ru(0001) interface. An intercalation mechanism was suggested in which the intercalating species penetrate under the graphene sheets through the open edges of graphene islands. By DFT calculations, Na and Si migration through graphene were investigated previously.^{22,23} It was concluded

Received: June 4, 2018

Revised: September 14, 2018

Published: September 18, 2018

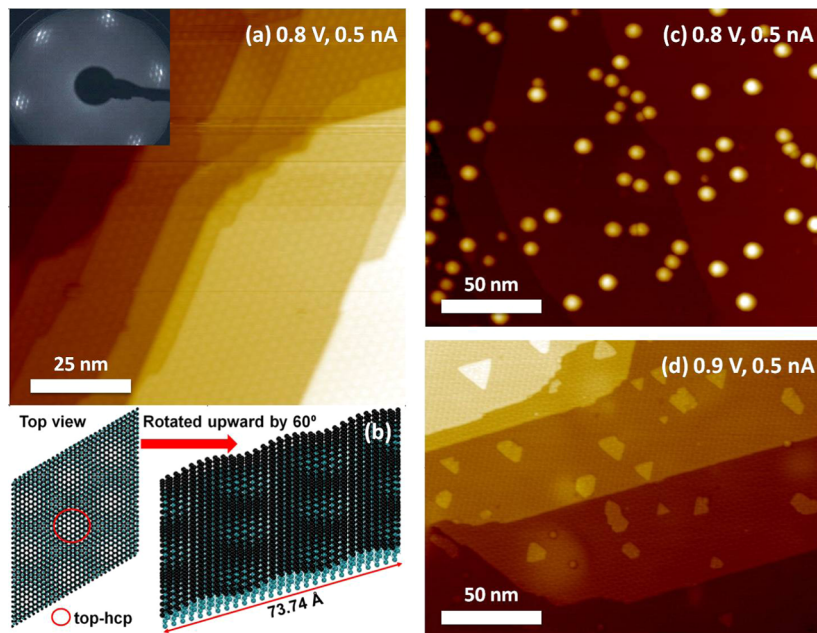


Figure 1. (a) STM (and LEED) image of the as-prepared graphene grown on Ru(0001), the LEED pattern is shown in the inset. (b) DFT-derived structural model of monolayer graphene on Ru(0001). (c) STM image of Fe deposited on graphene/Ru(0001) at room temperature. (d) STM image taken at room temperature after annealing (c) at 700 K.

that the intercalation of Na and Si atoms requires atomic defects in the graphene lattice. The defect-penetrating process of Li and Cu atoms through zero-layer graphene (ZLG), the remaining C atoms near the surface forming a distorted graphene layer, on SiC(0001) has been theoretically studied, and it was proposed that Li and Cu atoms can enter ZLG through defects such as eight-membered rings and double vacancies, respectively.^{20,24} The intercalation of Pd atoms into graphene/Ru(0001) interface was studied based on model calculations, and Pd was assumed to induce defects in graphene at high temperatures.²⁵

In this work, we chose Ru(0001) as the substrate because a continuous monolayer graphene of highly ordered crystalline structure can be prepared by thermal annealing.²⁶ We studied the intercalation process of Fe, which is of potential scientific and technological importance because the graphene covered Fe islands could possibly be used as arrays of magnetic nanostructures with chemical stability toward oxidation in air. We observed the Fe intercalation experimentally and explored the mechanism of the process using the DFT calculation.

2. METHODS

2.1. Experimental Methods. The experiments were carried out in an ultrahigh vacuum (UHV) chamber (base pressure 1×10^{-10} mbar) equipped with low-energy electron diffraction (LEED), Auger electron spectroscopy, infrared reflection–adsorption spectroscopy (IRAS), scanning tunneling microscopy (STM), and a quadrupole mass spectrometer for temperature-programmed desorption. The Ru(0001) crystal was mounted on an Omicron sample holder. The temperature was measured by a Type K thermocouple spot-welded to the edge of the crystal. A clean Ru(0001) surface was obtained by cycles of Ar⁺ sputtering at 300 K and annealing in UHV to 1400 K. The well-ordered graphene layer was prepared by annealing the sample at 1200 K for 5 min to let carbon atoms segregate from the Ru bulk and accumulate on the surface.²⁶ Fe (99.99%) was deposited using an e-beam

assisted evaporator (EMT3, Omicron). The substrate was kept at 300 K during deposition and a typical Fe deposition rate of 0.3 monolayer per min was used. The STM, LEED, and IRAS measurements were performed at 300 K. A bias was applied on the sample for STM measurements.

2.2. Computational Methods. All the calculations were carried out using the Perdew–Burke–Ernzerhof (PBE²⁷) functional and projector-augmented wave potential,^{28,29} as implemented in the Vienna ab initio simulation package.^{30,31} The long-range van der Waals interactions were accounted for by means of the Grimme GGA-type functional (PBE-D3).³² The cutoff energy was set to 400 eV and transition state (TS) structures were estimated using the CI-NEB procedure.³³ A major issue in the interfacial calculation is the accommodation of the mismatch between the Ru and graphene lattices. To relieve the stress on a major part of the atoms, we used a (10 × 10) graphene sheet over a (9 × 9) Ru(0001) supercell with two layers and a vacuum region 15.0 Å in width, where the top layer including surface species was relaxed and the bottom layer was fixed in bulk position. The surface structure relaxation and the total energy calculation were performed with a Monkhorst–Pack *k*-point mesh of 1 × 1 × 1.

3. RESULTS AND DISCUSSION

Annealing the clean Ru(0001) crystal at 1200 K for 5 min results in an ordered graphene layer formed by carbon atoms segregated from the Ru bulk and accumulated on the surface.²⁶ The LEED (see inset in Figure 1a) shows a 1 × 1 pattern with additional spots, which are characteristic of a Moiré structure that is commonly observed for epitaxial layers having a lattice mismatch to a metal support. Each Moiré structure contains 12 carbon/11 Ru.^{26,34,35} In the STM image in Figure 1a, it is clearly visible that the film grows continuously and uniformly, exhibiting a Moiré structure of high quality. The presence of an ordered Moiré structure indicates that the graphene film is a monolayer rather than a bilayer, as the latter does not exhibit a Moiré structure with a long-range order.³⁶ Figure 1b shows the

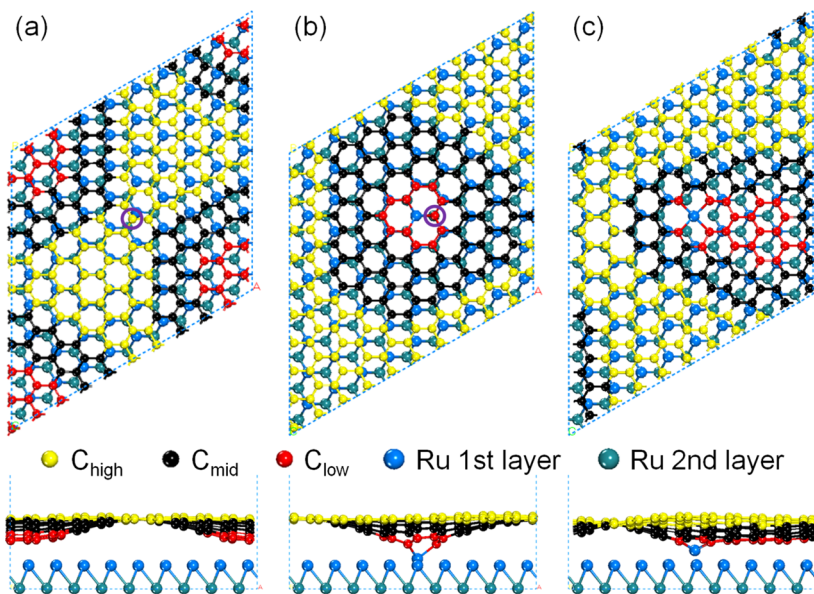


Figure 2. Schematic top (up) and side (down) views of the periodical model surface structures of Ru(0001)-supported perfect graphene (a) and defective graphene with monovacancies (b) or bivacancies (c).

optimized atomic-structure model of a monolayer graphene on Ru(0001) derived by DFT, where the Moiré structure is consistent with the observation in the experiments and the height of the variation (0.1556 nm) is slightly larger than the reported value observed in STM (0.11 nm).³⁵

As shown in Figure 1c, depositing Fe at 300 K on a graphene film grown on Ru(0001) results in Fe particles, which are imaged with a diameter between 4 and 10 nm and a height of 1.2 and 2.5 nm, which is in good agreement with the clustering of Fe that occurs at room temperature due to the diffusion of the Fe adatoms during the deposition process. It has been reported that lattice defects and domain boundaries in graphene act as nucleation centers.¹⁷ In our STM results, we have only observed lattice defects (see in Figure S1 marked with black dash circle) but no obvious multiple domains of graphene; therefore, we conclude that the Fe particles shown in Figure 1c are located on the defect sites of the graphene layer.

The STM image after annealing to 700 K in Figure 1d shows that the Fe particles transform into two-dimensional (2D) islands with an apparent height ~ 0.2 nm, which indicates that the Fe island is a layer of monoatomic thickness, and a Moiré structure on the surface. This phenomenon has been observed by many research groups and the thus formed 2D islands are interpreted as metal intercalated into the interface of the graphene and the substrate, such as Ni and Pd on graphene/Ru(0001) by Jin et al.²¹ and Ni and Fe on graphene/Rh(111) by Sicot et al.^{17,23} We therefore conclude that the Fe atoms penetrate the graphene layer and intercalate into the graphene/Ru(0001) interface after annealing at 700 K. The density of the 2D Fe islands formed after annealing is less than the as-deposited Fe particles, which may be caused by some of the Fe atoms moving away from the original nucleation sites during annealing at elevated temperature.

Following our previous assumption that the initial Fe particles are anchored to the defect sites in the graphene layer, we suggest that these sites also play a role in the intercalation process in which the Fe atoms have to cross the graphene layer to reach the underlying Ru surface. This rationale motivates

our choice to study the dynamics of the intercalation process in more detail using DFT.

Generally, graphene may contain various types of defects;³⁷ here, we limit ourselves to defective graphene containing carbon vacancies, two representative defect models, graphene with monovacancies (graphene-MV), and graphene with bivacancies (graphene-BV). Figure 2 displays the top and side views of the optimized structures of perfect graphene, graphene-MV, and graphene-BV on a Ru(0001) surface with a (9×9) unit cell and a slab of two layers, containing 162 Ru atoms and 200 carbon atoms. Figure 2b shows the optimized structure from Figure 2a with the C-atom in the purple circle taken away to create a carbon vacancy. The carbon atom that was removed to create the vacancy was originally located far away from the Ru substrate; however, the unsaturated neighboring carbon atoms around the carbon vacancy coordinate strongly with the underlying Ru substrate after removing the C atom. The side view of this system shows that a Ru atom is pulled out of the Ru surface plane by the C atoms, which possess dangling bonds due to the creation of the C-vacancy. A bivacancy graphene layer was created by removing an additional carbon atom (marked with a purple circle in Figure 2b) adjacent to the first vacancy. The optimized structure shown in Figure 2c presents a 5–8–5 ring, a structure that was observed in the zero-layer graphene formed on SiC surfaces.²⁰ The side view in Figure 2c shows that the Ru atom coordinating to the C-atoms adjacent to the bivacancy is pulled out even further compared to the system with a single vacancy. This result is similar to the conclusion given by Ugeda et al. that the defect site carbon atoms move out of the graphene plane toward Pt(111) substrate to form chemical bonds that results in decrease in the distance between graphene and Pt substrate.³⁸

Dispersing the Fe adatom on graphene layers on Ru(0001), DFT optimization results show that the Fe atom binds strongly on the defect sites, with the adsorption energies of -4.88 , -6.64 , and -7.55 eV on perfect graphene and graphene-MV and graphene-BV on Ru(0001), respectively, referencing to iron in the bulk.

The nudged-elastic band approach was used to study the energetics of Fe intercalation into the interface between graphene-MV and the flat Ru(0001) surface. Figure 3 shows

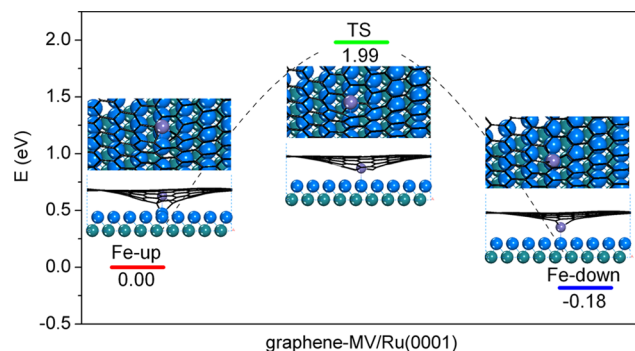


Figure 3. DFT-calculated energy diagram as well as structures of IS, TS, and FS for one Fe atom intercalation into graphene-MV/Ru(0001) (first layer Ru/blue; second layer Ru/green; Fe/purple; C/black).

the optimized initial state (IS), the transition state, and the final state (FS) structures and their relative energies with respect to the initial state. The barrier (E_a) and the reaction energy (E_r) are calculated according to $E_a = E_{TS} - E_{IS}$ and $E_r = E_{FS} - E_{IS}$, where E_{IS} , E_{TS} , and E_{FS} are the total energies of the corresponding initial state (IS), transition state (TS), and final state (FS), respectively. The process is computed to be exothermic by 0.18 eV. The distances between C and Fe in the computed transition state (TS) structure (1.711, 1.711, and 1.714 Å) are shorter than those in the initial state (IS) (1.816, 1.816, and 1.817 Å) and the final state (FS) (1.748, 1.748, and 1.751 Å), indicating a repulsive interaction between C and Fe in the transition state (TS), which results in a barrier of 1.99 eV. This result explains the necessity of annealing the sample to an elevated temperature, 700 K in our experiment, to trigger the Fe intercalation process. It is worth mentioning that without considering the van der Waals interactions between the graphene layer and the Ru(0001) substrate (Figure S2), the barrier for intercalation is only 0.70 eV, which would imply that the interaction would happen already at about room temperature, which is inconsistent with our experimental

results. Therefore, the inclusion of van der Waals interactions is necessary for an accurate description of this system.

Next, we considered the intercalation process of two Fe atoms in the system with one vacancy in the graphene lattice. As shown in Figure 4, when Fe dimer is restricted to adsorb above the graphene plane, inclining toward the graphene-MV (Figure 4b) is slightly stable by 0.04 eV than upright on the defect (Figure 4a). We found that the energy of the structure with one of the Fe atoms sitting above the graphene plane and another Fe located at the interface of the graphene layer and the Ru substrate (Figure 4c) is 1.02 eV lower than the one in Figure 4a. After both Fe atoms have intercalated (Figure 4d), the relative energy decreases further to a value 2.52 eV lower than the one in Figure 4a. It is clear that the intercalation process of an iron dimer into the graphene-MV/Ru(0001) interface is thermodynamically favored. It is worth noting that the energy change in the Fe dimer intercalation is more than twice the energy of the single-Fe-atom intercalation. In addition, the local structure of the carbon vacancy can be influenced by the number of Fe atoms, such as the hole size of the defect shown in Figure 4a is 6 per cent larger than the one with a single Fe atom above graphene-MV/Ru(0001). This agrees with the previously published experimental data, which show that metal adatoms can induce major structural reconstruction of graphene.^{39,40} Therefore, the intercalation process may become easier with increasing numbers of Fe adatoms.

We furthermore considered Fe penetration through a graphene layer with bivacancy on the (9 × 9) Ru(0001) surface, graphene-BV. As shown in Figure 5a, the Fe atom above the defect of graphene-BV intercalates to graphene-BV and Ru substrate interface (Figure 5b) without barrier and releases 0.57 eV of heat. This differs from the situation of the Fe atom penetrating through a single vacancy in graphene, in which case, a barrier of 1.99 eV was found. We therefore conclude that the intercalation of Fe through a double carbon vacancy in the graphene layer is kinetically easier than when there is only a single carbon vacancy.

For the Fe dimer, shown in Figure 6a, we find that it adopts a tilted geometry when restricted above the graphene layer, thereby bonding with multiple carbon atoms surrounding the double vacancy. The energy of the structure with one Fe atom above graphene-BV and another below graphene-BV (as

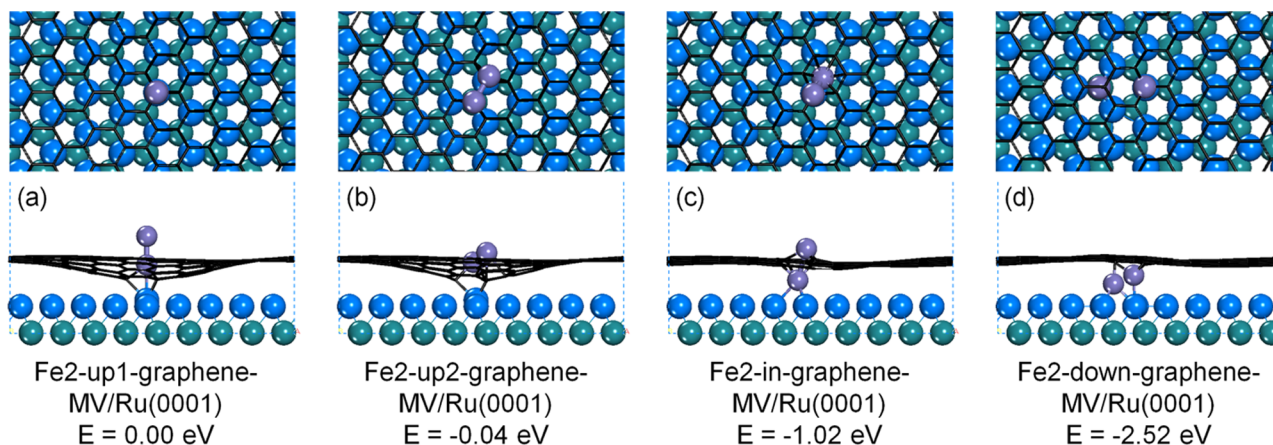


Figure 4. Optimized structures and energies (E) of two Fe atoms (a) upright on defect, (b) leaning on the graphene-MV, (c) one Fe above the graphene and the other Fe located at the interface, and (d) both Fe atoms intercalated. Energy is depicted as the relative total energy (in eV) to Fe₂-up1-graphene-MV/Ru(0001).

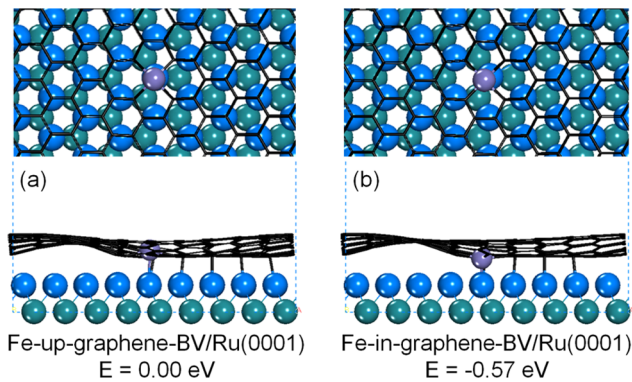


Figure 5. Optimized structures and energies (E) for the cases of single iron adatom (a) above and (b) underneath the graphene layer. Energy is depicted as the relative total energy (in eV) to (a) Fe-up-graphene-BV/Ru(0001).

shown in Figure 6b), which can be considered as an intermediate of the intercalation process, is 0.30 eV higher than the structure in Figure 6a. The second Fe atom intercalation has no barrier and causes 1.62 eV energy drop. When both Fe atoms locate in the graphene/Ru(0001) interface, where we believe that the intercalation process is finished, the total energy of this structure is 1.32 eV less than the initial situation, Figure 6a. Thus, we conclude that Fe intercalation into graphene-BV/Ru(0001) is thermodynamically favored.

It is important to note that for both defective graphene with monocarbon vacancy and bicarbon vacancy, the energy of the system after intercalation did not change much compared to the initial structure, where the Fe atom was located on top of the graphene layer. In contrast, when adding another Fe to form a dimer, the energy change of the intercalation is more significant. Therefore, we can draw the conclusion that more the number of Fe atoms are involved, more the intercalation process becomes thermodynamically favored. To examine this conclusion, we further calculated the intercalation process of Fe trimer. For graphene-MV (see in Figure 7), two final situations have been considered: first, the energy change is -3.43 eV when all three Fe atoms are located close to the C vacancy after intercalation, second, the energy change is -3.76 eV when two Fe atoms in the Fe trimer move away from the defect site and leave one Fe atom bond to the carbon atoms, thereby stabilizing the defect. The energy change in the intercalation of a Fe trimer is -2.43 eV for graphene-BV (see

in Figure S3). The DFT-calculated energies (E_{DFT} , eV), total relative energies ΔE (eV), and relative energies per Fe atom $\Delta E'$ (eV/Fe atom) for the intercalation systems are summarized in Table S1. These results further confirm the conclusion that the involvement of more Fe atoms results in the intercalation processes being more thermodynamically favored. To understand the interaction between Fe and the Gr/Ru before and after intercalation, calculation of the differential electron densities ($\Delta\rho$) were carried out. Compared with the Fe trimer upright on graphene (Figure 8a), $\Delta\rho$ for the Fe located at the interface (Figure 8b) shows a larger increase in electron density (red regions) between Fe and Ru. This result illustrates the stronger interaction between Fe and Ru than the one between Fe and graphene, which is the driving force of intercalation.

The above-presented experimental and DFT results provide a compelling evidence that the intercalation of Fe into graphene/Ru(0001) interfaces is thermodynamically favored. The experimental results show that the intercalation occurs at elevated temperatures, 700 K, suggesting the penetration of the Fe through the graphene layer is associated with an energy barrier. This conclusion is concurrent with the calculation results showing that one Fe atom going through a defect with one carbon vacancy to the interface between graphene and Ru(0001) substrate faces an energy barrier of 1.99 eV. Based on the comparison of the calculation results of one Fe atom on MV- and BV-graphene/Ru(0001), we conclude that the intercalation becomes easier with increasing number of carbon vacancies at a defect site, which can be explained by the increasing pore size of the defect with more missing neighboring carbon atoms in the graphene structure. Another trend is that it is more thermodynamically favored for the intercalation process when more Fe atoms are involved, for instance, on MV-graphene/Ru(0001), the system with one Fe atom releases 0.18 eV of heat, that with Fe dimer releases 2.52 eV, and that with Fe trimer releases 3.43 or 3.76 eV depending on Fe atom location after intercalation; similarly, on BV-graphene/Ru(0001), the system releases 0.57, 1.32, and 2.43 eV of heat for one Fe atom, Fe dimer, and Fe trimer, respectively. The driving force of the intercalation is the stronger interaction between Fe and Ru than the one between Fe and graphene.

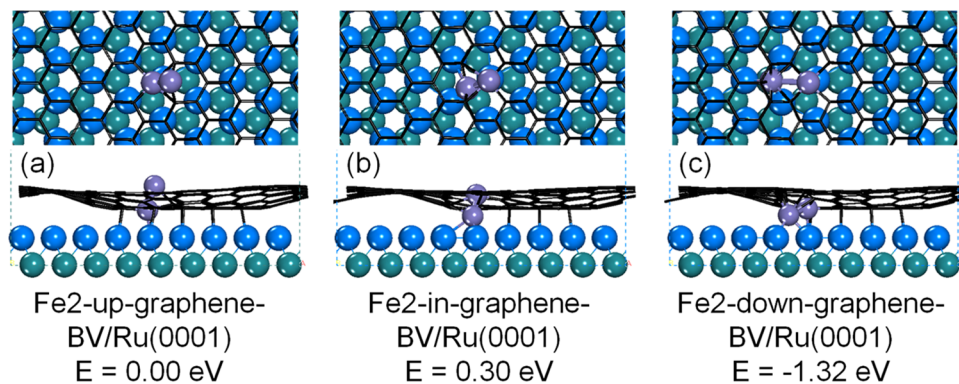


Figure 6. DFT-calculated energy diagram as well as structures for two Fe atom intercalation into graphene-BV/Ru(0001). Both Fe atoms are above the graphene layer (a), one Fe atom is above the graphene layer and another is at the interface (b), and both Fe atoms are at the interface (c).

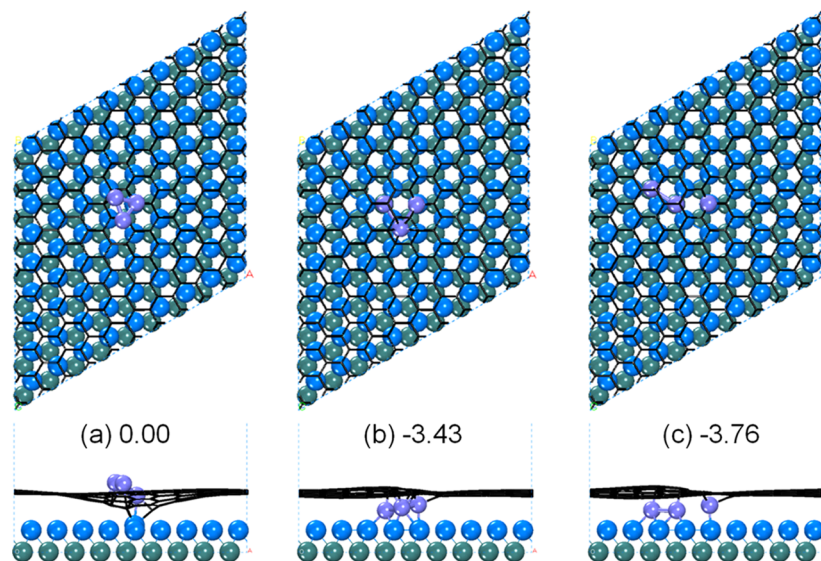


Figure 7. Optimized structures and energies of the Fe trimer (a) upright on the defect of the graphene-MV and located at the interface (b, c). Energy is depicted as the relative total energy (in eV) to (a).

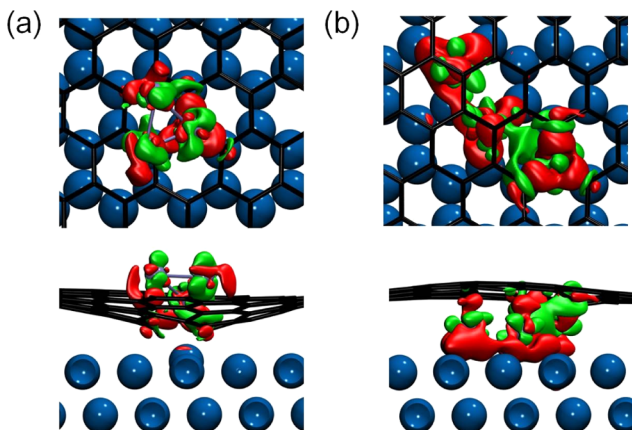


Figure 8. Isosurface (isovalue = 0.04 au) of differential electron density ($\Delta\rho$) for Fe trimer (a) upright on the defect of the graphene-MV (corresponding to Figure 7a) and (b) located at the interface (corresponding to Figure 7c). The $\Delta\rho$ is defined as $\Delta\rho = \rho_{\text{total}} - \rho_{\text{Gr/Ru}} - \rho_{\text{Fe}}$. Ru and Fe atoms are represented by dark and light blue lines and graphene by black lines. The red and green regions indicate the increase and decrease of electron density, respectively.

4. CONCLUSIONS

In summary, we have studied the Fe intercalation on graphene/Ru(0001) systems both experimentally and computationally with the aim to better understand the process of intercalation. Based on our results, several conclusions can be drawn: the intercalation of Fe into graphene/Ru(0001) interface is thermodynamically favored with certain energy barriers, such as 1.99 eV for one Fe atom on graphene-MV/Ru(0001); the penetration of Fe through the graphene layer is easier when increasing the carbon vacancy at the defect site; and increasing the Fe atom number results in the intercalation process becoming more thermodynamically favored. The electronic structure analysis illustrates that the stronger interaction between Fe and Ru than the one between Fe and graphene is the driving force of intercalation.

With this work, we provide insight into the Fe intercalation in graphene/substrate systems and hope these conclusions may be of general importance for the field of graphene technology.

■ ASSOCIATED CONTENT

Supporting Information

The Supporting Information is available free of charge on the ACS Publications website at DOI: [10.1021/acs.jpcc.8b05370](https://doi.org/10.1021/acs.jpcc.8b05370).

STM image of the as-prepared graphene grown on Ru(0001) (Figure S1); DFT-calculated energy diagram as well as structures of IS, TS, and FS for one Fe atom intercalation into graphene-MV/Ru(0001) without the long-range van der Waals interactions corrections (Figure S2); optimized structures and energies of the Fe tripolymer upright on defect of the graphene-BV and located at the interface (Figure S3) ([PDF](#))

■ AUTHOR INFORMATION

Corresponding Authors

*E-mail: wxd@sxicc.ac.cn (X.W.).

*E-mail: yuxin@synfuelschina.com.cn (X.Y.).

ORCID

Pengju Ren: [0000-0003-3752-1638](https://orcid.org/0000-0003-3752-1638)

C. J. Kees-Jan Weststrate: [0000-0003-4346-166X](https://orcid.org/0000-0003-4346-166X)

Xiaodong Wen: [0000-0001-5626-8581](https://orcid.org/0000-0001-5626-8581)

Xin Yu: [0000-0002-8390-4034](https://orcid.org/0000-0002-8390-4034)

Notes

The authors declare no competing financial interest.

■ ACKNOWLEDGMENTS

This work is partially supported by the National Natural Science Foundation of China (Nos 21603253, 21473229, and 91545121) and Beijing Talents Foundation (No. 2017000021223ZK17). We acknowledge the Hundred-Talent Program of the Chinese Academy of Sciences, Shanxi Hundred-Talent Program and National Thousand Young Talents Program of China. The computational resources for the project were supplied by the Tianhe-2 in Lvliang, Shanxi. We also acknowledge helpful discussions with Dr Xiong Zhou,

Dr Gilbere Mannie, Dr Tingbin Lim, and Dr Tianfu Zhang. Syngaschem BV acknowledges significant funding by Synfuels China Technology, Co. Ltd.

■ REFERENCES

- (1) Tombros, N.; Jozsa, C.; Popinciuc, M.; Jonkman, H. T.; van Wees, B. J. Electronic Spin Transport and Spin Precession in Single Graphene Layers at Room Temperature. *Nature* **2007**, *448*, 571–574.
- (2) Karpan, V. M.; Giovannetti, G.; Khomyakov, P. A.; Talanana, M.; Starikov, A. A.; Zwierzycki, M.; van den Brink, J.; Brocks, G.; Kelly, P. J. Graphite and Graphene as Perfect Spin Filters. *Phys. Rev. Lett.* **2007**, *99*, No. 176602.
- (3) Giovannetti, G.; Khomyakov, P. A.; Brocks, G.; Karpan, V. M.; van den Brink, J.; Kelly, P. J. Doping Graphene with Metal Contacts. *Phys. Rev. Lett.* **2008**, *101*, No. 026803.
- (4) Lu, J.; Fu, B. S.; Kung, M. C.; Xiao, G. M.; Elam, J. W.; Kung, H. H.; Stair, P. C. Coking- and Sintering-Resistant Palladium Catalysts Achieved through Atomic Layer Deposition. *Science* **2012**, *335*, 1205–1208.
- (5) Besenbacher, F.; Chorkendorff, I.; Clausen, B. S.; Hammer, B.; Molenbroek, A. M.; Norskov, J. K.; Stensgaard, I. Design of a Surface Alloy Catalyst for Steam Reforming. *Science* **1998**, *279*, 1913–1915.
- (6) Wintterlin, J.; Bocquet, M. L. Graphene on Metal Surfaces. *Surf. Sci.* **2009**, *603*, 1841–1852.
- (7) Batzill, M. The Surface Science of Graphene: Metal Interfaces, CVD Synthesis, Nanoribbons, Chemical Modifications, and Defects. *Surf. Sci. Rep.* **2012**, *67*, 83–115.
- (8) Weststrate, C. J.; Kizilkaya, A. C.; Rossen, E. T. R.; Verhoeven, M. W. G. M.; Ciobica, I. M.; Saib, A. M.; Niemantsverdriet, J. W. Atomic and Polymeric Carbon on Co(0001): Surface Reconstruction, Graphene Formation, and Catalyst Poisoning. *J. Phys. Chem. C* **2012**, *116*, 11575–11583.
- (9) Kim, K. S.; Zhao, Y.; Jang, H.; Lee, S. Y.; Kim, J. M.; Kim, K. S.; Ahn, J.-H.; Kim, P.; Choi, J.-Y.; Hong, B. H. Large-Scale Pattern Growth of Graphene Films for Stretchable Transparent Electrodes. *Nature* **2009**, *457*, 706–710.
- (10) Bae, S.; Kim, H.; Lee, Y.; Xu, X.; Park, J.-S.; Zheng, Y.; Balakrishnan, J.; Lei, T.; Kim, H. R.; Song, Y. I.; et al. Roll-to-Roll Production of 30-Inch Graphene Films for Transparent Electrodes. *Nat. Nanotech.* **2010**, *5*, 574–578.
- (11) Karpan, V. M.; Giovannetti, G.; Khomyakov, P. A.; Talanana, M.; Starikov, A. A.; Zwierzycki, M.; van den Brink, J.; Brocks, G.; Kelly, P. J. Graphite and Graphene as Perfect Spin Filters. *Phys. Rev. Lett.* **2007**, *99*, No. 176602.
- (12) Maassen, J.; Ji, W.; Guo, H. Graphene Spintronics: The Role of Ferromagnetic Electrodes. *Nano Lett.* **2011**, *11*, 151–155.
- (13) Tontegode, A. Y. Carbon on Transition Metal Surfaces. *Prog. Surf. Sci.* **1991**, *38*, 201–429.
- (14) Shikin, A. M.; Prudnikova, G. V.; Adamchuk, V. K.; Moresco, F.; Rieder, K.-H. Surface Intercalation of Gold Underneath a Graphite Monolayer on Ni(111) Studied by Angle-Resolved Photoemission and High-Resolution Electron-Energy-Loss Spectroscopy. *Phys. Rev. B* **2000**, *62*, 13202–13208.
- (15) Dedkov, Y. S.; Shikin, A. M.; Adamchuk, V. K.; Molodtsov, S. L.; Laubschat, C.; Bauer, A.; Kaindl, G. Intercalation of Copper Underneath a Monolayer of Graphite on Ni(111). *Phys. Rev. B* **2001**, *64*, No. 035405.
- (16) Riedl, C.; Coletti, C.; Iwasaki, T.; Zakharov, A. A.; Starke, U. Quasi-Free-Standing Epitaxial Graphene on SiC Obtained by Hydrogen Intercalation. *Phys. Rev. Lett.* **2009**, *103*, No. 246804.
- (17) Sicot, M.; Leicht, P.; Zusan, A.; Bouvron, S.; Zander, O.; Weser, M.; Dedkov, Y. S.; Horn, K.; Fonin, M. Size-Selected Epitaxial Nanoislands Underneath Graphene Moiré on Rh(111). *ACS Nano* **2012**, *6*, 151–158.
- (18) Sutter, P.; Sadowski, J. T.; Sutter, E. A. Chemistry under Cover: Tuning Metal–Graphene Interaction by Reactive Intercalation. *J. Am. Chem. Soc.* **2010**, *132*, 8175–8179.
- (19) Cui, Y.; Gao, J.; Jin, L.; Zhao, J.; Tan, D.; Fu, Q.; Bao, X. An Exchange Intercalation Mechanism for the Formation of a Two-Dimensional Si Structure Underneath Graphene. *Nano Res.* **2012**, *5*, 352–360.
- (20) Orimoto, Y.; Otsuka, K.; Yagyu, K.; Tochihara, H.; Suzuki, T.; Aoki, Y. Theoretical Study of Cu Intercalation through a Defect in Zero-Layer Graphene on SiC Surface. *J. Phys. Chem. C* **2017**, *121*, 7294–7302.
- (21) Jin, L.; Fu, Q.; Yang, Y.; Bao, X. A Comparative Study of Intercalation Mechanism at Graphene/Ru(0001) Interface. *Surf. Sci.* **2013**, *617*, 81–86.
- (22) Yang, S.; Li, S.; Tang, S.; Shen, D.; Dong, W.; Sun, W. Adsorption, Intercalation and Diffusion of Na on Defective Bilayer Graphene: Computational Study. *Surf. Sci.* **2017**, *658*, 31–37.
- (23) Sicot, M.; Bouvron, S.; Zander, O.; Rüdiger, U.; Dedkov, Y. S.; Fonin, M. Nucleation and Growth of Nickel Nanoclusters on Graphene Moiré on Rh(111). *Appl. Phys. Lett.* **2010**, *96*, No. 093115.
- (24) Li, Y.; Zhou, G.; Li, J.; Wu, J.; Gu, B.-L.; Duan, W. Lithium Intercalation Induced Decoupling of Epitaxial Graphene on SiC(0001): Electronic Property and Dynamic Process. *J. Phys. Chem. C* **2011**, *115*, 23992–23997.
- (25) Huang, L.; Pan, Y.; Pan, L.; Gao, M.; Xu, W.; Que, Y.; Zhou, H.; Wang, Y.; Du, S.; Gao, H.-J. Intercalation of Metal Islands and Films at the Interface of Epitaxially Grown Graphene and Ru(0001) Surfaces. *Appl. Phys. Lett.* **2011**, *99*, No. 163107.
- (26) Pan, Y.; Zhang, H.; Shi, D.; Sun, J.; Du, S.; Liu, F.; Gao, H. Highly Ordered, Millimeter-Scale, Continuous, Single-Crystalline Graphene Monolayer Formed on Ru(0001). *Adv. Mater.* **2008**, *20*, 1–4.
- (27) Perdew, J. P.; Burke, K.; Ernzerhof, M. Generalized Gradient Approximation Made Simple. *Phys. Rev. Lett.* **1996**, *77*, 3865–3868.
- (28) Blöchl, P. E. Projector Augmented-Wave Method. *Phys. Rev. B* **1994**, *50*, 17953–17979.
- (29) Kresse, G.; et al. From Ultrasoft Pseudopotentials to the Projector Augmented-Wave Method. *Phys. Rev. B* **1999**, *59*, 1758–1775.
- (30) Kresse, G.; Furthmüller, J. Efficiency of Ab-initio Total Energy Calculations for Metals and Semiconductors Using a Plane-Wave Basis Set. *Comput. Mater. Sci.* **1996**, *6*, 15–50.
- (31) Kresse, G.; Furthmüller, J. Efficient Iterative Schemes for Ab initio Total-Energy Calculations Using a Plane-Wave Basis Set. *Phys. Rev. B* **1996**, *54*, 11169–11186.
- (32) Grimme, S.; Antony, J.; Ehrlich, S.; Krieg, S. A Consistent and Accurate Ab Initio Parametrization of Density Functional Dispersion Correction (DFT-D) for the 94 Elements H–Pu. *J. Chem. Phys.* **2010**, *132*, No. 154104.
- (33) Henkelman, G.; Jónsson, H. Improved Tangent Estimate in the Nudged Elastic Band Method for Finding Minimum Energy Paths and Saddle Points. *J. Chem. Phys.* **2000**, *113*, 9978–9985.
- (34) de Parga, A. L. V.; Calleja, F.; Borca, B.; Passeggi, M. C. G.; Hinarejos, J. J.; Guinea, F.; Miranda, R. Periodically Rippled Graphene: Growth and Spatially Resolved Electronic Structure. *Phys. Rev. Lett.* **2008**, *100*, No. 056807.
- (35) Marchini, S.; Günther, S.; Wintterlin, J. Scanning tunneling microscopy of graphene on Ru(0001). *Phys. Rev. B* **2007**, *76*, No. 075429.
- (36) Sutter, E.; Acharya, D. P.; Sadowski, J. T.; Sutter, P. Scanning tunneling microscopy on epitaxial bilayer graphene on ruthenium(0001). *Appl. Phys. Lett.* **2009**, *94*, No. 133101.
- (37) Banhart, F.; Kotakoski, J.; Krasheninnikov, A. V. Structural Defects in Graphene. *ACS Nano* **2011**, *5*, 26–41.
- (38) Ugeda, M. M.; Fernández-Torre, D.; Brihuega, I.; Pou, P.; Martínez-Galera, A. J.; Pérez, R.; Gómez-Rodríguez, J. M. Point Defects on Graphene on Metals. *Phys. Rev. Lett.* **2011**, *107*, No. 116803.
- (39) Ci, L.; Xu, Z.; Wang, L.; Gao, W.; Ding, F.; Kelly, K. F.; Yakobson, B. I.; Ajayan, P. M. Controlled nanocutting of graphene. *Nano Res.* **2008**, *1*, 116–122.

(40) Datta, S. S.; Strachan, D. R.; Khamis, S. M.; Johnson, A. T. C. Crystallographic Etching of Few-Layer Graphene. *Nano Lett.* **2008**, *8*, 1912–1915.